

# Low-Discrepancy Points via Energetic Variational Inference

Yindong Chen, Yiwei Wang<sup>\*</sup>, Lulu Kang<sup>†</sup> and Chun Liu

Department of Applied Mathematics, Illinois Institute of Technology

## Abstract

In this paper, we propose a deterministic variational inference approach and generate low-discrepancy points by minimizing the kernel discrepancy, also known as the Maximum Mean Discrepancy or MMD. Based on the general energetic variational inference framework (Wang et al., 2021), minimizing the kernel discrepancy is transformed to solving a dynamic ODE system via the explicit Euler scheme. We name the resulting algorithm EVI-MMD and demonstrate it through examples in which the target distribution is fully specified, partially specified up to the normalizing constant, and empirically known in the form of training data. Its performances are satisfactory compared to alternative methods in the applications of distribution approximation, numerical integration, and generative learning. The EVI-MMD algorithm overcomes the bottleneck of the existing MMD-descent algorithms, which are mostly applicable to two-sample problems. Algorithms with more sophisticated structures and potential advantages can be developed under the EVI framework.

**Keywords:** Approximate Bayesian Inference, Kernel Discrepancy, Generative Learning, Maximum Mean Discrepancy (MMD), Numerical Integration, Variational Inference.

## 1 Introduction

Many methods in statistics, machine learning, and applied mathematics require the generation of samples from a certain target distribution. For example, in Bayesian statistics, the most crucial step is to sample from the posterior distribution of the unknown parameters. In this case, the target distribution is often partially known without the scaling constant. Numerical integration is another important tool used in many computational solutions in finance, engineering, science, etc. It approximates the multidimensional integration  $I = \mathbb{E}_{\mathbf{x} \sim \mu}[f(\mathbf{X})] = \int_{\Omega} f(\mathbf{x})\mu(d\mathbf{x})$  by the sample mean  $\hat{I}_n = \frac{1}{N} \sum_{i=1}^N f(\mathbf{x}_i)$ , where the  $f(\mathbf{x})$  is the integral function,  $\mu$  is the probability measure with the support region  $\Omega$ , and  $\mathbf{x}_i$ 's are the i.i.d. samples following the distribution of  $\mu$ . For numerical integration, the target distribution is fully specified. Statistical design of experiments is also related to this area. One such instance is the uniform space-filling design (Fang et al., 2000), in which the design points should approximate the uniform distribution. Broadly speaking, many supervised and unsupervised learning tasks involve the problem of generating samples from a distribution. Only in this case, the target distribution is an empirical distribution from the observation data. Among these tasks, generative learning models (Harshvardhan et al., 2020) have gained a lot of attention and popularity due to the wide application of generative adversarial networks (or GANs) (Creswell et al., 2018; Goodfellow et al., 2014) and variational autoencoders (or VAE) (Kingma

<sup>\*</sup>Yindong Chen and Yiwei Wang share the first authorship due to equal contribution.

<sup>†</sup>Lulu Kang is the corresponding author. lkang2@iit.edu

and Welling, 2013). The essential task of generative learning is to generate new samples from the empirical distribution of training data in a parametric or nonparametric fashion.

In recent decades, variational inference (VI) has become an important and popular tool in machine learning, statistics, applied mathematics (Jordan et al., 1999; Wibisono et al., 2016a; Blei et al., 2017; Mnih and Rezende, 2016; Gorbach et al., 2018), etc. In short, the main goal of a VI method is to generate samples to approximate a target distribution. Naturally, VI is strongly tied to these aforementioned research areas. First and foremost, variational Bayesian inference (Fox and Roberts, 2012; Blei et al., 2017) is an alternative to the classic MCMC approach to approximate a posterior distribution. Compared with classic MCMC, VI methods are less computationally intensive and thus more suitable to analyze large datasets and can be used whenever there is a need to explore many models (Blei et al., 2006). The core idea of a VI approach is to convert the inference problem into an optimization problem by minimizing a certain dissimilarity functional that measures the difference between any distribution and the posterior distribution. Its drawback, compared to MCMC, is that the minimal solution is not guaranteed to converge to the posterior distribution, which depends on many aspects including the distribution family, i.e., the feasible region of the minimization. Despite so, its computational advantage has propelled the development of many VI-based supervised and unsupervised learning methods, such as Bayesian neural networks (Graves, 2011; Louizos and Welling, 2017; Wu et al., 2019; Shridhar et al., 2019), Gaussian process model (King and Lawrence, 2006; Nguyen and Bonilla, 2013, 2014; Shetha et al., 2015; Damianou et al., 2016; Cheng and Boots, 2017), and generative learning models (Kingma et al., 2014; Hu et al., 2018).

In this paper, we propose a new variational inference approach by minimizing the kernel discrepancy via the energetic variational approach (Wang et al., 2021). Essentially, we generate samples, or *particles* using the more conventional wording in VI, to approximate various target distributions that are fully specified, partially specified up to the normalizing constant, or empirically available from data. In Quasi-Monte Carlo (QMC), the low-discrepancy sequence is the sequence that leads to a small kernel discrepancy value so as to approximate the uniform distribution, such as Sobol sequences (Sobol, 1976). Usually, such sequences are computed sequentially following an explicit formula (Caffisch, 1998). Inspired by the low-discrepancy sequence, we name the particles generated by the proposed variational approach *low-discrepancy points*. We use the word “points” instead of “sequence” to imply that the points are not generated sequentially and are not just for uniform distribution.

## 1.1 Related Works

As mentioned above, the core idea of VI is to minimize a user-specified dissimilarity functional that measures the difference between two distributions. Many dissimilarity functionals, such as Kullback–Leibler (KL-)divergence and the more general  $f$ -divergence (Csiszár et al., 2004; Zhang et al., 2019), Wasserstein distance (Villani, 2021), kernel stein discrepancy (KSD) (Liu et al., 2016; Chen et al., 2018b), and the more general kernel discrepancy, have been used in the literature.

If the target distribution is known up to the intractable normalizing constant, KL-divergence is commonly used (Liu and Wang, 2016; Blei et al., 2017; Ma et al., 2019; Heng et al., 2021). For example, the Langevin Monte Carlo (LMC) (Welling and Teh, 2011; Cheng et al., 2018; Bernton, 2018) and the Stein Variational Gradient Descent (SVGD) (Liu and Wang, 2016) can be considered as a discretization of the Wasserstein gradient flow (Jordan et al., 1998) of the KL-divergence. However, KL-divergence is only suitable for the target distribution whose density function takes the form  $\frac{1}{Z} \exp(-V(\mathbf{x}))$ . Moreover, the KL-divergence based algorithms require repeated evaluation of the gradient of the target distribution, which can be computationally costly if the target distribution

is complicated to compute.

Kernel discrepancy is another popular dissimilarity functional. In machine learning, kernel discrepancy is better known as *Maximum Mean Discrepancy* or *MMD*. It is suitable to the cases where the target distribution is compactly supported or the target is only known in the form of training data (Li et al., 2015, 2017). Besides, minimizing MMD does not require the repeated evaluation of the density of the target distribution. For these reasons, we choose the kernel discrepancy or MMD as the objective functional. We defer the detailed review of kernel discrepancy/MMD and its related literature in Section 2.

Another important aspect of a VI approach is the minimization method. As reviewed by Blei et al. (2017), the complexity of the minimization is largely decided by the distribution family  $\mathcal{Q}$ , i.e., the set of feasible distributions to approximate the target distribution. It can be a family of parametric distributions. If independence assumption is properly imposed, mean-field approach and coordinate descent can be used (Blei et al., 2017) for minimization. Sometimes, the parametric distribution is too restrictive, and thus flow-based VI methods have been created, in which  $\mathcal{Q}$  consists of distributions obtained by a series of smooth transformations from a tractable initial reference distribution. Examples include normalizing flow VI methods (Rezende and Mohamed, 2015; Kingma et al., 2016; Salman et al., 2018) and particle-based VI methods (ParVIs) (Liu and Wang, 2016; Liu, 2017; Liu and Zhu, 2017; Chen et al., 2018a; Liu et al., 2019; Chen et al., 2019; Wang et al., 2021). The proposed approach belongs to the ParVIs category. Among all the ParVIs, SVGD (Liu, 2017) is one of the most popular early works and we also choose it for comparison.

## 1.2 Our Contributions

In this paper, we propose a deterministic method of generating a set of low-discrepancy points that minimizes the kernel discrepancy via the general energetic variational inference (EVI) framework (Wang et al., 2021). Compared to some existing works that also minimize MMD, the proposed approach applies to many scenarios, including the cases when the target distribution is fully known, partially known up to the normalizing constant, or empirically given by the data, whereas most existing MMD methods (Gretton et al., 2012; Li et al., 2015; Liu et al., 2016; Li et al., 2017; Mak and Joseph, 2018; Cheng and Xie, 2021; Hofert et al., 2021) focus on the two-sample problem, in which the target distribution is not given but only training data are available. It can explain why most of the referred methods are applied to generative learning models.

Another contribution is the combination of the EVI framework with the MMD functional. As shown in Section 3 and discussed in Section 5, EVI transforms the minimization problem into a dynamic system, which can be solved by many different numerical schemes. Due to limited space, we only choose the simplest explicit Euler scheme for illustration.

The rest of the paper is organized as follows. Section 2 gives the necessary background on the kernel discrepancy and the EVI framework. In Section 3, we apply the general EVI framework to minimize the kernel discrepancy and obtain a dynamic ODE system to update the particles iteratively. Using the explicit Euler numerical scheme to solve this ODE system, we introduce the EVI-MMD algorithm. In Section 4, three numerical examples are used to compare the proposed approach with some competitors. We conclude the paper with a discussion on the extension of the proposed approach in Section 5.

## 2 Background

We first review the concept of kernel discrepancy, which is better known as MMD in machine learning literature, and then explain the EVI framework. The two combined are the foundation of

the proposed low-discrepancy points generation method.

## 2.1 Kernel Discrepancy or MMD

Before its wide recognition in machine learning as MMD, kernel discrepancy has been an important concept in QMC literature and was promoted as a goodness-of-fit statistic and a quality measure for statistical experimental design by many works in the '90s and early 2000, such as [Hickernell \(1998, 1999\)](#); [Fang et al. \(2000\)](#); [Fang and Mukerjee \(2000\)](#); [Fang et al. \(2002\)](#); [Hickernell and Liu \(2002\)](#). One of the main reasons that kernel discrepancy is so influential in so many different areas is that it can be interpreted in different ways. [Hickernell \(2016\)](#) and [Li et al. \(2020\)](#) explained *three identities* of kernel discrepancy. First, it can be considered as a norm on a Hilbert space of measures, which has to include the Dirac measure. Second, it is commonly used as a deterministic cubature error bound for Monte Carlo methods. Third, it is the root mean squared cubature error, where the kernel function is also the covariance function for a stochastic process. Here we review it using the second identity and then generalize it and connect it with MMD.

Let  $\Omega \subset \mathbb{R}^d$  be the domain of a probability measure  $\mu$ , which has density  $\rho(\mathbf{x})$  and cumulative distribution function  $F(\mathbf{x})$ . The three concepts, measure, density, and CDF, are used interchangeably in the rest of the paper to refer to distribution. Let  $(\mathcal{H}, \langle \cdot, \cdot \rangle_{\mathcal{H}})$  be a reproducing kernel Hilbert space (RKHS) of functions  $f : \Omega \rightarrow \mathbb{R}$ . By definition, the reproducing kernel,  $K$ , is the unique function defined on  $\Omega \times \Omega$  with the properties that  $K(\cdot, \mathbf{x}) \in \mathcal{H}$  for any  $\mathbf{x} \in \Omega$  and  $f(\mathbf{x}) = \langle K(\cdot, \mathbf{x}), f \rangle_{\mathcal{H}}$ . The second property implies that  $K$  reproduces function values via the inner product. It can be verified that  $K$  is symmetric in its arguments and positive definite.

A cubature method approximates the integral  $I = \int_{\Omega} f(\mathbf{x})\rho(\mathbf{x})d\mathbf{x} = \mathbb{E}_{\mathbf{x} \sim \mu}[f(\mathbf{X})]$  of an  $f \in \mathcal{H}$  by the sample mean

$$\hat{I}_N = \frac{1}{N} \sum_{i=1}^N f(\mathbf{x}_i), \quad \text{where } \mathbf{x}_i \sim^{iid} F(\mathbf{x}).$$

Let  $\mathcal{X} = \{\mathbf{x}_i\}_{i=1}^N$  be the set of the i.i.d. samples following  $F(\mathbf{x})$  distribution. To measure the quality of the approximation, define the cubature error as

$$\text{err}(f, \mathcal{X}) = I - \hat{I}_N = \int_{\Omega} f(\mathbf{x})\rho(\mathbf{x})d\mathbf{x} - \frac{1}{N} \sum_{i=1}^N f(\mathbf{x}_i) = \int_{\Omega} f(\mathbf{x})d[F(\mathbf{x}) - F_{\mathcal{X}}(\mathbf{x})],$$

where  $F_{\mathcal{X}}$  is the empirical CDF based on the sample  $\mathcal{X}$ . Under modest assumptions of the reproducing kernel, based on Cauchy-Schwarz inequality, the tight, worst-case cubature error bound is

$$|\text{err}(f, \mathcal{X})| \leq \|f\|_{\mathcal{H}} D(\mathcal{X}, F, K),$$

where  $\|f\|_{\mathcal{H}}$  is the norm of the function  $f$  based on the inner product of the RKHS  $\mathcal{H}$  and  $D(\mathcal{X}, F, K)$  is the kernel discrepancy whose square is equal to

$$\begin{aligned} D^2(\mathcal{X}, F, K) &= \int_{\Omega \times \Omega} K(\mathbf{x}, \mathbf{y})d[F(\mathbf{x}) - F_{\mathcal{X}}(\mathbf{x})]d[F(\mathbf{y}) - F_{\mathcal{X}}(\mathbf{y})] \\ &= \int_{\Omega \times \Omega} K(\mathbf{x}, \mathbf{y})dF(\mathbf{x})dF(\mathbf{y}) - \frac{2}{N} \sum_{i=1}^N \int_{\Omega} K(\mathbf{x}_i, \mathbf{y})dF(\mathbf{y}) + \frac{1}{N^2} \sum_{i,j=1}^N K(\mathbf{x}_i, \mathbf{x}_j). \end{aligned} \quad (1)$$

Recall that the kernel discrepancy is also the norm on a Hilbert space of measures, i.e., the first identity mentioned earlier. More specifically, this Hilbert space of measures, denoted by  $\mathcal{M}$ , is the

closure of the pre-Hilbert space and its inner product is defined as

$$\langle \nu_1, \nu_2 \rangle_{\mathcal{M}} = \int_{\Omega \times \Omega} K(\mathbf{x}, \mathbf{y}) \nu_1(d\mathbf{x}) \nu_2(d\mathbf{y}).$$

For the given kernel  $K$ , the Hilbert space contains all measures such that  $\|\nu\|_{\mathcal{M}}$  is bounded. Please see [Hickernell \(2016\)](#) or [Li et al. \(2020\)](#) for the detailed definitions of the RKHS  $\mathcal{H}$ ,  $\mathcal{M}$ , and the derivation of (1).

To make sure the cubature error is small for any function  $f \in \mathcal{H}$ ,  $\mathcal{X}$  should minimize the discrepancy  $D^2(\mathcal{X}, F, K)$ , i.e., have a low discrepancy. Based on the above definitions, we formally introduce low-discrepancy points.

**Definition 1** (Low-discrepancy points). *For any given measure  $\mu \in \mathcal{M}$ , the set of low-discrepancy points with respect to  $\mu$  is defined as*

$$\mathcal{X}^* = \{\mathbf{x}_i^*\}_{i=1}^N = \arg \min_{\mathcal{X} \subset \Omega} D^2(\mathcal{X}, F, K), \quad (2)$$

where  $F$  is the CDF corresponding to  $\mu$ .

The kernel discrepancy can be more generally defined by

$$D^2(\nu_1, \nu_2, K) = \int_{\Omega \times \Omega} K(\mathbf{x}, \mathbf{y}) [\nu_1(d\mathbf{x}) - \nu_2(d\mathbf{x})] [\nu_1(d\mathbf{y}) - \nu_2(d\mathbf{y})], \quad (3)$$

measuring the difference between any  $\nu_1, \nu_2 \in \mathcal{M}$ . [Gretton et al. \(2012\)](#) defined the maximum mean discrepancy (MMD) as

$$\text{MMD}(\mathcal{H}, \nu_1, \nu_2) = \sup_{f \in \mathcal{H}} (\mathbb{E}_{\mathbf{x} \sim \nu_1} [f(\mathbf{x})] - \mathbb{E}_{\mathbf{y} \sim \nu_2} [f(\mathbf{y})]),$$

and under the same definition of  $\mathcal{H}$  and  $\mathcal{M}$ , the square of MMD is

$$\text{MMD}^2(\mathcal{H}, \nu_1, \nu_2) = \mathbb{E}_{\mathbf{x}, \mathbf{x}' \sim \nu_1} [K(\mathbf{x}, \mathbf{x}')] - 2\mathbb{E}_{\mathbf{x} \sim \nu_1, \mathbf{y} \sim \nu_2} [K(\mathbf{x}, \mathbf{y})] + \mathbb{E}_{\mathbf{y} \sim \nu_2, \mathbf{y}' \sim \nu_2} [K(\mathbf{y}, \mathbf{y}')],$$

which is equivalent to  $D^2(\nu_1, \nu_2, K)$  in (3). Therefore, in the rest of the paper, we use kernel discrepancy and MMD interchangeably.

Kernel discrepancy has many desirable properties, one of which is on the convergence of distributions. In fact,  $\text{MMD}(\mathcal{H}, \nu_1, \nu_2) = 0$  if and only if  $\nu_1 = \nu_2$ , provided that  $\Omega$  is a compact metric space and more importantly,  $K$  is a universal kernel and thus  $\mathcal{H}$  is a universal RKHS ([Gretton et al., 2012](#)). Simply put, universal kernel ([Micchelli et al., 2006](#)) means that  $K$  has to be complex enough such that  $\mathcal{H}$  and  $\mathcal{M}$  are sufficiently big. Lower-order polynomial kernels, such as linear and second-order polynomials are not universal. MMD induced by the second-order polynomial kernel can distinguish two distributions in terms of mean and variance, and the linear kernel can only do so in terms of the mean. On the other hand, the Gaussian kernel is universal and thus the MMD based on it can be used as a metric for measures ([Micchelli et al., 2006](#); [Fukumizu et al., 2007](#)). Therefore, with a proper kernel, if  $D^2(\mathcal{X}_N, F, K) \rightarrow 0$  as  $N \rightarrow \infty$ , then  $F_{\mathcal{X}_N} \rightarrow F$ . For fixed  $N$ , if  $D^2(\mathcal{X}, F, K) \rightarrow 0$  as  $n \rightarrow \infty$  ( $n$  is the notation for iteration of algorithm), then  $F_{\mathcal{X}} \rightarrow F$ . Kernel discrepancy is also related to energy statistics ([Székely and Rizzo, 2013](#)) and support points ([Mak and Joseph, 2018](#)). If let  $K(\mathbf{x}, \mathbf{y}) = \|\mathbf{x} - \mathbf{y}\|_2^2$ , then the kernel discrepancy becomes energy statistics and thus low-discrepancy points become support points.

## 2.2 Energetic Variational Inference

Motivated by the energetic variational approaches for modeling the dynamics of non-equilibrium thermodynamical systems (Giga et al., 2017), the energetic variational inference (EVI) framework uses a continuous energy-dissipation law to specify the dynamics of minimizing the objective function in machine learning problems. Under the EVI framework, a practical algorithm can be obtained by introducing a suitable discretization to the continuous energy-dissipation law. This idea was introduced and applied to variational inference by Wang et al. (2021). It can also be applied to other machine learning problems similarly to Trillos and Sanz-Alonso (2020) and E et al. (2020).

We first introduce the EVI using the continuous formulation. Let  $\phi_t$  be the dynamic flow map  $\phi_t : \mathbb{R}^d \rightarrow \mathbb{R}^d$  that continuously transforms the  $d$ -dimensional distribution from an initial distribution toward the target one and we require the map  $\phi_t$  to be smooth and one-to-one. The functional  $\mathcal{F}(\phi_t)$  is a user-specified divergence or other machine learning objective functional, such as the KL-divergence in Wang et al. (2021). Taking analogy of a thermodynamics system,  $\mathcal{F}(\phi_t)$  is the Helmholtz free energy. Following the First and Second Law of thermodynamics (Giga et al., 2017) (kinetic energy is set to be zero)

$$\frac{d}{dt}\mathcal{F}(\phi_t) = -\Delta(\phi_t, \dot{\phi}_t), \quad (4)$$

where  $\Delta(\phi_t, \dot{\phi}_t)$  is a user-specified functional representing the rate of energy dissipation, and  $\dot{\phi}_t$  is the derivative of  $\phi_t$  with time  $t$ . So  $\dot{\phi}_t$  can be interpreted as the “velocity” of the transformation. Each variational formulation gives a natural path of decreasing the objective functional  $\mathcal{F}(\phi_t)$  toward an equilibrium.

The dissipation functional should satisfy  $\Delta(\phi_t, \dot{\phi}_t) \geq 0$  so that  $\mathcal{F}(\phi_t)$  decreases with time. As discussed in Wang et al. (2021), there are many ways to specify  $\Delta(\phi_t, \dot{\phi}_t)$  and the simplest among them is a quadratic functional in terms of  $\dot{\phi}_t$ ,

$$\Delta(\phi_t, \dot{\phi}_t) = \int_{\Omega_t} \rho_{[\phi_t]} \|\dot{\phi}_t\|_2^2 dx,$$

where  $\rho_{[\phi_t]}$  denotes the pdf of the current distribution which is the initial distribution transformed by  $\phi_t$ ,  $\Omega_t$  is the current support, and  $\|\mathbf{a}\|_2 = \mathbf{a}^\top \mathbf{a}$  for  $\forall \mathbf{a} \in \mathbb{R}^d$ . This simple quadratic functional is appealing since it has a simple functional derivative, i.e.,

$$\frac{\delta \Delta(\phi_t, \dot{\phi}_t)}{\delta \dot{\phi}_t} = 2\rho_{[\phi_t]} \dot{\phi}_t,$$

where  $\delta$  is the variation operator, i.e., functional derivative.

With the specified energy-dissipation law (4), the energy variational approach derives the dynamics of the systems through two variational procedures, the Least Action Principle (LAP) and the Maximum Dissipation Principle (MDP), which leads to

$$\frac{\delta \frac{1}{2} \Delta}{\delta \dot{\phi}_t} = -\frac{\delta \mathcal{F}}{\delta \phi_t}.$$

The approach is motivated by the seminal works of Raleigh (Rayleigh, 1873) and Onsager (Onsager, 1931a,b). Using the quadratic  $\mathcal{D}(\phi_t, \dot{\phi}_t)$ , the dynamics of decreasing  $\mathcal{F}$  is

$$\rho_{[\phi_t]} \dot{\phi}_t = -\frac{\delta \mathcal{F}}{\delta \phi_t}. \quad (5)$$



In general, this continuous formulation is difficult to solve, since the manifold of  $\phi_t$  is of infinite dimension. Naturally, there are different approaches to approximate an infinite-dimensional manifold by a finite-dimensional manifold. One such approach, as used in Wang et al. (2021), is to use particles (or samples) to approximate the continuous distribution  $\rho_{[\phi_t]}$  with kernel regularization. If this approximation applies to (5), after the LAP and MDP variational steps, we call it the “variation-then-approximation” approach. If this approximation is applied to (4) directly, before any variational steps, we call it the “approximation-then-variation” approach. The latter leads to a discrete version of the energy-dissipation law, i.e.,

$$\frac{d}{dt}\mathcal{F}_h(\{\mathbf{x}_i(t)\}_{i=1}^N) = -\Delta_h(\{\mathbf{x}_i(t)\}_{i=1}^N, \{\dot{\mathbf{x}}_i(t)\}_{i=1}^N). \quad (6)$$

Here  $\{\mathbf{x}(t)\}_{i=1}^N$  is the locations of  $N$  particles at time  $t$  and  $\dot{\mathbf{x}}_i(t)$  is the derivative of  $\mathbf{x}_i$  with  $t$ , and thus is the velocity of the  $i$ th particle as it moves toward the target distribution. The subscript  $h$  of  $\mathcal{F}$  and  $\Delta$  denotes the bandwidth parameter of the kernel function used in the kernelization operation. Applying the variational steps to (6), we obtain the dynamics of decreasing  $\mathcal{F}$  at the particle level,

$$\frac{\delta \frac{1}{2}\Delta_h}{\delta \dot{\mathbf{x}}_i(t)} = -\frac{\delta \mathcal{F}_h}{\delta \mathbf{x}_i}, \quad \text{for } i = 1, \dots, N. \quad (7)$$

This leads to an ODE system of  $\{\mathbf{x}_i(t)\}_{i=1}^N$  and can be solved by different numerical schemes. The solution is the particles approximating the target distribution.

Due to limited space, we can only briefly review the EVI framework and explain it intuitively. Readers can find the rigorous and concrete explanation in Wang et al. (2021). It also suggested many different ways to specify the energy-dissipation, the ways to approximate the continuous formulation and different ways to solve the ODE system.

### 3 Low-Discrepancy Points via EVI

In this section, we first apply the EVI framework to minimize the kernel discrepancy and derive the ODE system of the particles and then introduce the EVI-MMD algorithm which uses the explicit Euler method to discretize the ODEs in time and the AdaGrad algorithm to decide the step size. The EVI-MMD algorithm solves the ODE system and generates the low-discrepancy points. We also discuss the choice of the kernel function and how to adjust outliers from the initial distribution.

#### 3.1 EVI-MMD

Given the target probability measure  $\mu$  whose CDF is  $F$ , and the proper reproducing kernel, we choose the squared kernel discrepancy  $D^2(\mathcal{X}_N, F, K)$  defined in (1) as the Helmholtz free energy and the quadratic dissipation functional to set up the energy-dissipation law. Specifically,

$$\mathcal{F}_h(\{\mathbf{x}_i(t)\}_{i=1}^N) = D^2(\{\mathbf{x}_i(t)\}_{i=1}^N, F, K), \quad \Delta_h(\{\mathbf{x}_i(t)\}_{i=1}^N, \{\dot{\mathbf{x}}_i(t)\}_{i=1}^N) = \frac{1}{N} \sum_{i=1}^N \|\dot{\mathbf{x}}_i(t)\|_2^2. \quad (8)$$

For the kernel discrepancy defined in (1), which directly compares the empirical distribution of  $\mathcal{X}_N$  and  $F$ , using the approximation-then-variation makes more sense since the free energy is already approximated by  $N$  particles. Based on these setup, the discrete energy-dissipation law for the low-discrepancy points is

$$\frac{d}{dt}D^2(\{\mathbf{x}_i(t)\}_{i=1}^N, F, K) = -\frac{1}{N} \sum_{i=1}^N \|\dot{\mathbf{x}}_i(t)\|_2^2. \quad (9)$$

Next, we need to derive of variation of  $D^2(\{\mathbf{x}_i(t)\}_{i=1}^N, F, K)$  and  $\frac{1}{N} \sum_{i=1}^N \|\dot{\mathbf{x}}_i(t)\|_2^2$  with respect to  $\mathbf{x}_i$  and  $\dot{\mathbf{x}}_i$ , respectively.

$$\frac{\delta \frac{1}{2} \Delta_h}{\delta \dot{\mathbf{x}}_i} = \frac{1}{N} \dot{\mathbf{x}}_i(t), \quad (10)$$

$$\frac{\delta \mathcal{F}_h}{\delta \mathbf{x}_i} = \frac{2}{N^2} \sum_{k \neq i}^N [\nabla_{\mathbf{x}} K(\mathbf{x}_i, \mathbf{x}_k)] - \frac{2}{N} \int_{\Omega} [\nabla_{\mathbf{x}} K(\mathbf{x}_i, \mathbf{y})] dF(\mathbf{y}). \quad (11)$$

The derivation of the two variations are included in Appendix A1. Following (7), we obtain the ODE system (12) that provides the dynamics of minimizing  $D^2(\{\mathbf{x}_i(t)\}_{i=1}^N, F, K)$ .

$$\dot{\mathbf{x}}_i(t) = 2 \int_{\Omega} [\nabla_{\mathbf{x}} K(\mathbf{x}_i, \mathbf{y})] dF(\mathbf{y}) - \frac{2}{N} \sum_{k \neq i}^N [\nabla_{\mathbf{x}} K(\mathbf{x}_i, \mathbf{x}_k)], \quad \text{for } i = 1, \dots, N. \quad (12)$$

Note that the gradient  $\nabla_{\mathbf{x}} K(\mathbf{x}, \mathbf{y})$  is applied to  $\mathbf{x}$  of the kernel. We choose a symmetric kernel function as in most machine learning methods, i.e.,  $K(\mathbf{x}, \mathbf{y}) = K(\mathbf{y}, \mathbf{x})$ . Particularly, if  $K(\mathbf{x}, \mathbf{y})$  takes the radial basis function  $K(\mathbf{x}, \mathbf{y}) = r(\|\mathbf{x} - \mathbf{y}\|_2)$  with a certain positive function  $r(\cdot)$ , then  $\nabla_{\mathbf{x}} K(\mathbf{x}, \mathbf{y}) = -\nabla_{\mathbf{y}} K(\mathbf{x}, \mathbf{y})$ .

There are two terms on the right side of (12). Intuitively, the first term  $\int_{\Omega} [\nabla_{\mathbf{x}} K(\mathbf{x}_i, \mathbf{y})] dF(\mathbf{y})$  can be interpreted as a *driving force* that guides particles towards the target distribution, and the second term  $\frac{1}{N} \sum_{k \neq i}^N [\nabla_{\mathbf{x}} K(\mathbf{x}_i, \mathbf{x}_k)]$  is a *repulsive force* to stop particles from collapsing. We have borrowed this interpretation from Ba et al. (2019) and the authors interpreted the stein variational gradient descent (SVGD) and MMD-descent in the same way. The SVGD and MMD-descent share some similar structures with (12). We will remark the difference between the proposed EVI-MMD and MMD-descent in Section 3.2. Also, in Section 3.2, we will discuss how to easily compute the integration in the driving force term.

A practical algorithm can be obtained by solving the ODE system numerically. Indeed, most optimization algorithms can be viewed as an approximation of a continuous ODE or SDE, which in turn provides a theoretical foundation of these optimization methods (Cheng et al., 2018; Wibisono et al., 2016b). In this paper, we adopt the simplest explicit Euler discretization to the ODE (12), which leads to

$$\mathbf{x}_i^{n+1} = \mathbf{x}_i^n - \tau_n \mathbf{v}_i^n, \quad i = 1, 2, \dots, N. \quad (13)$$

where  $\tau_n$  is the step size of the  $n$ th iteration, and

$$\mathbf{v}_i^n = \left( \frac{2}{N} \sum_{k \neq i}^N [\nabla_{\mathbf{x}} K(\mathbf{x}_i^n, \mathbf{x}_k^n)] - 2 \int_{\Omega} [\nabla_{\mathbf{x}} K(\mathbf{x}_i^n, \mathbf{y})] dF(\mathbf{y}) \right). \quad (14)$$

Interestingly, the explicit Euler discretization turns out to be the standard gradient descent of the kernel discrepancy.

A drawback of the explicit Euler approach is that the step size has to be small so that the algorithm converges to the true solution with stability as long as some modest conditions on convergence are satisfied. On the other hand, small step size can lead to long iteration until convergence and thus make the algorithm less efficient. To overcome this dilemma between stability and efficiency, we use the AdaGrad (Adaptive Gradient) algorithm (Duchi et al., 2011) to determine the step size. The AdaGrad updates each particle  $\mathbf{x}_i$  as follows,

$$\mathbf{x}_i^{n+1} = \mathbf{x}_i^n - \eta_t \mathbf{v}_i^n, \quad (15)$$

$$\eta_t = \eta_0 \text{diag}[\mathbf{G}_i^n + \epsilon_0 \mathbf{I}_d]^{-\frac{1}{2}}. \quad (16)$$



Here  $\boldsymbol{\eta}_t$  is commonly called *learning rate* in machine learning. It is a diagonal matrix that updates the step size in the direction of  $\mathbf{v}_i^n$  elementwise, which is an improvement to the constant step size  $\tau_n$  for all elements of  $\mathbf{v}_i^n$  in the explicit Euler. The scalar  $\eta_0$  is the initial learning rate, a user-specified tuning parameter. The matrix  $\mathbf{G}_i^n$  is  $\mathbf{G}_i^n = \sum_{j=1}^n \mathbf{v}_i^j (\mathbf{v}_i^j)^\top$  and  $\mathbf{I}_d$  is the identity matrix of the same size. Adding  $\epsilon_0 \mathbf{I}_d$  to  $\mathbf{G}_i$  is to regularize  $\mathbf{G}_i^n$  to avoid singularity. Note that updating the learning rate via (16) only needs the diagonal entry of  $\mathbf{G}_i^n$ . So a less computational way to update  $\boldsymbol{\eta}_t$  is

$$\boldsymbol{\eta}_t = \eta_0 \text{diag} \left[ \left( \sum_{j=1}^n (v_{i,1}^j)^2 + \epsilon_0 \right)^{-1/2}, \dots, \left( \sum_{j=1}^n (v_{i,d}^j)^2 + \epsilon_0 \right)^{-1/2} \right], \quad (17)$$

where the operation  $\text{diag}$  makes the  $d$  elements into a diagonal matrix. Applying other numerical schemes to solve the ODE system, such as the implicit Euler (Wang et al., 2021), will lead to different optimization algorithms. We will explore this in the future.

### 3.2 Kernel Function

The remaining question is how to compute the integration contained in the driving force term. If the target distribution  $F(\mathbf{y})$  is given by the training data  $\{\mathbf{y}_k\}_{k=1}^M$  as in the two-sample problem, the driving force term can be computed directly by

$$\mathbb{E}_{\mathbf{y} \sim F}[\nabla_{\mathbf{x}} K(\mathbf{x}_i, \mathbf{y})] = \int \nabla_{\mathbf{x}} K(\mathbf{x}_i, \mathbf{y}) dF(\mathbf{y}) = \frac{1}{M} \sum_{k=1}^M \nabla_{\mathbf{x}} K(\mathbf{x}_i, \mathbf{y}_k) \quad (18)$$

for  $i = 1, \dots, N$ . In this case, many different types of symmetric and positive definite kernels can be used. In practice, if  $M$  is too large, we can randomly sample a subset of training data to estimate each  $\mathbb{E}_{\mathbf{y} \sim F}[\nabla_{\mathbf{x}} K(\mathbf{x}_i, \mathbf{y})]$ .

We discuss the case when the target distribution is given analytically. It becomes a trivial problem if the target distribution is a known distribution and easy to sample from. Otherwise, it is a challenging problem to estimate the driving force term efficiently. To solve this problem, we look into the term  $\mathbb{E}_{\mathbf{y} \sim F}[\nabla_{\mathbf{x}} K(\mathbf{x}, \mathbf{y})]$  more closely for any  $\mathbf{x}$ . Let  $\rho(\mathbf{y})$  be the pdf of  $F(\mathbf{y})$ . If  $K(\mathbf{x}, \mathbf{y})$  is the Gaussian kernel,  $K(\mathbf{x}, \mathbf{y}) = \exp\left(-\frac{\|\mathbf{x} - \mathbf{y}\|_2^2}{2h^2}\right)$ , then its gradient is

$$\nabla_{\mathbf{x}} K(\mathbf{x}, \mathbf{y}) = -\frac{\mathbf{x} - \mathbf{y}}{h^2} \exp\left(-\frac{\|\mathbf{x} - \mathbf{y}\|_2^2}{2h^2}\right). \quad (19)$$

Then the integration of the gradient of the kernel is

$$\int_{\Omega} \nabla_{\mathbf{x}} K(\mathbf{x}, \mathbf{y}) \rho(\mathbf{y}) d\mathbf{y} = \int_{\Omega} -\frac{\mathbf{x} - \mathbf{y}}{h^2} \exp\left(-\frac{\|\mathbf{x} - \mathbf{y}\|_2^2}{2h^2}\right) \rho(\mathbf{y}) d\mathbf{y}. \quad (20)$$

If  $\Omega = \mathbb{R}^d$ , the integration becomes the following

$$\int_{\mathbb{R}^d} \nabla_{\mathbf{x}} K(\mathbf{x}, \mathbf{y}) \rho(\mathbf{y}) d\mathbf{y} = (\sqrt{2\pi}h)^d \mathbb{E}_{\mathbf{y}} \left[ -\frac{\mathbf{x} - \mathbf{y}}{h^2} \rho(\mathbf{y}) \right], \quad (21)$$

where the expectation is with respect to  $\mathbf{y}$  following the normal distribution  $\mathcal{N}(\mathbf{x}, h^2 \mathbf{I}_d)$ . If  $\Omega \subsetneq \mathbb{R}^d$ , we can still use (21) to approximate  $\int_{\Omega} \nabla_{\mathbf{x}} K(\mathbf{x}, \mathbf{y}) \rho(\mathbf{y}) d\mathbf{y}$  because the bandwidth parameter  $h$  is typically much smaller compared to the scale of  $\Omega$  (to be discussed next) and the probability mass

outside of  $\Omega$  is negligible. To sum up, if we choose Gaussian kernel, we can estimate the driving force term by the following cubature,

$$\mathbb{E}_{\mathbf{y} \sim F(\mathbf{y})}[\nabla_{\mathbf{x}} K(\mathbf{x}_i, \mathbf{y})] \approx -(\sqrt{2\pi}h)^d \frac{1}{L} \sum_{l=1}^L \frac{\mathbf{x}_i - \mathbf{y}_l}{h^2} \rho(\mathbf{y}_l), \quad (22)$$

where  $\mathbf{y}_l$  for  $l = 1, \dots, L$  are iid samples following  $\mathcal{N}(\mathbf{x}_i, h^2 \mathbf{I}_d)$ . In practice, we can first generate  $L \times d$  samples  $y_{l,k}$  from the univariate  $\mathcal{N}(0, h^2)$  for  $k = 1, \dots, d$  and shift the mean of  $\mathbf{y}_l$  to  $\mathbf{x}_i$  to reduce the computational costs. Alternatively, to reduce the bias of the samples from a single batch, we can generate  $L$  samples in each iteration for each  $\mathbf{x}_i$ . Considering both accuracy and efficiency, we choose the latter approach and set  $L = 200$  in the numerical examples.

One can see that this idea applies to other universal kernel functions as long as its gradient  $\nabla_{\mathbf{x}} K(\mathbf{x}, \mathbf{y})$  is proportional to a known pdf and is also easy to sample from. Other than the Gaussian kernel, exponential kernel (or Laplacian kernel) also meets these conditions. Since the Gaussian kernel is one of the most widely used kernel functions in machine learning, we choose the Gaussian kernel in the numerical examples. To facilitate the description of the algorithm, we define the terms representing the driving and repulsive force for each of the particle in the  $n$ th iteration as follows.

$$\text{driving}_i^n = -\frac{2(\sqrt{2\pi}h)^d}{L} \sum_{l=1}^L \frac{\mathbf{x}_i^n - \mathbf{y}_l}{h^2} \rho(\mathbf{y}_l), \quad (23)$$

$$\text{repulsive}_i^n = -\frac{2}{N} \sum_{k \neq i}^N \frac{\mathbf{x}_i^n - \mathbf{x}_k^n}{h^2} \exp\left(-\frac{\|\mathbf{x}_i^n - \mathbf{x}_k^n\|_2^2}{2h^2}\right). \quad (24)$$

Then the gradient  $\mathbf{v}_i^n$  in (14) and (15) is  $\mathbf{v}_i^n = \text{repulsive}_i^n - \text{driving}_i^n$ .

As in most ParVI methods, the performance of the EVI-MMD algorithm is affected by the tuning parameter  $h$ . So far, there has not been a clear guideline in the literature on how to choose  $h$  to minimize MMD. For SVGD, [Liu and Wang \(2016\)](#) suggested using the median trick, i.e., set  $h^2 = \text{med}^2 / \log N$ , where med is the median of the pairwise distance between the particles in the current iteration. Therefore, the median trick updates  $h$  in each iteration. However, the median trick only works for SVGD. Some more sophisticated methods have been introduced to select  $h$  ([Liu et al., 2019](#); [Wang et al., 2019](#)) for SVGD. Despite these guidelines, choosing  $h$  still largely depends on the application. Most existing works select all the tuning parameters, including  $h$ , in a trial-and-error fashion.

In this paper, we set  $h$  to be a constant throughout the algorithm. First,  $h$  has to be sufficiently small. If  $h$  is too large, the driving force in (23) would be too small in size to have any “attraction” to move the particles toward the target distribution, and the repulsive force in (24) would be too small in size as well and cause the particles to collapse. The typical range of  $h$  should match the range of the pairwise distance between particles as suggested in [Peyré et al. \(2019\)](#). We can estimate this range from the initial distribution of the particles, then adjust its value based on multiple trials and choose the  $h$  value with the best result. Although *ad hoc*, this way of selecting  $h$  often performs better and more efficiently than the adaptive methods such as median trick in numerical experiments. This practice of fixing  $h$  is not rare in the VI literature. For example, [Li et al. \(2015\)](#) used a constant bandwidth parameter in the kernel function to train a deep generative model by minimizing MMD. The EVI-Im algorithm proposed in [Wang et al. \(2021\)](#) also sets  $h$  in this way. We choose other tuning parameters of the EVI-MMD algorithm in the trial-and-error fashion as well. These settings have performed reasonably well in many numerical studies we have conducted.

*Remark 1.* We want to compare the EVI-MMD with the existing MMD-descent approach. MMD-descent denotes the approach of applying gradient descent directly to MMD, which leads to

$$\frac{\mathbf{x}_i^{n+1} - \mathbf{x}_i^n}{\tau} = \Delta(\mathbf{x}_i^n) = -\mathbb{E}_{\mathbf{y} \sim F}[\nabla_{\mathbf{y}} K(\mathbf{x}_i^n, \mathbf{y})] + \frac{1}{N} \sum_{j=1}^N \nabla K_{\mathbf{x}_j}(\mathbf{x}_j^n, \mathbf{x}_i^n),$$

using the notation of this paper. One recent review on MMD-descent can be found in [Ba et al. \(2019\)](#). Ignoring the constant, this updating scheme is the same as the ODE system of EVI-MMD in (12). But EVI-MMD is fundamentally different from MMD-descent. First, EVI-MMD is originated from the EVI framework. Only using the combinations of these settings, simple quadratic dissipation law  $\Delta(\phi_t, \dot{\phi}_t) = \int_{\Omega_t} \rho_{[\phi_t]} \|\dot{\phi}_t\|^2 d\mathbf{x}$ , the “approximation-then-variation” order, and the explicit Euler scheme, the EVI-MMD would turn out to have the same updating formula as the MMD-descent. As suggested in [Wang et al. \(2021\)](#), other versions of EVI-MMD algorithms can be developed by choosing different dissipation functionals, switching the order of approximation and variation, and using implicit Euler or second-order numerical schemes to solve the ODE system. It is a future research direction we plan to pursue. Second, both EVI-MMD and MMD-descent face the same bottleneck, computing the driving force term. Our answer is estimating it by taking advantage of the Gaussian kernel. On the other hand, many MMD-descent methods bypass this problem via two options. The first option is only using MMD to solve a two-sample problem, in which the target distribution is given by the training data. So the driving force can be easily calculated using (18). This explains why MMD is mostly applied to the generative learning model, which is a two-sample problem. The second option is to use the Stein kernel based on the target distribution, then the driving force becomes

$$-\mathbb{E}_{\mathbf{y} \sim F}[\nabla_{\mathbf{y}} K(\mathbf{x}_i, \mathbf{y})] = \mathbb{E}_{\mathbf{y} \sim F}[\nabla_{\mathbf{y}} \log \rho(\mathbf{y}) K(\mathbf{x}, \mathbf{y})].$$

Without the context of the application, it is not possible to comment on which kernel is better, the Gaussian kernel or Stein kernel. Theoretically, this depends on which RKHS based on either kernel suits the application better. In terms of computational efficiency, this also depends on how easy it is to compute  $\mathbb{E}_{\mathbf{y} \sim F}[\nabla_{\mathbf{y}} \log \rho(\mathbf{y}) K(\mathbf{x}, \mathbf{y})]$ , which circles back to the same bottleneck problem if  $\rho(\mathbf{y})$  or  $F$  is not a known distribution.

### 3.3 Initial Outlier Detection and Adjustment

A drawback of using Gaussian kernels is that it can only capture the interaction between particles in a relatively small neighborhood, due to the fast decay of exponential function and small  $h$  value. During the early iterations of the algorithm, if a particle sits in a region where the density of the target distribution is small, in other words, the particle is an outlier to the target distribution, then the driving force  $\mathbb{E}_{\mathbf{y} \sim F}[\nabla_{\mathbf{x}} K(\mathbf{x}_i, \mathbf{y})]$  of this particle would be small in size. As a result, it would take more iterations to move this particle to the high-density region of the target distribution, or worse, the driving force is too small to make any significant movement and thus the particle remains an outlier when the algorithm terminates. In Appendix A2, we give a more rigorous explanation of the driving force term. To overcome the outlier issue, we propose a heuristic way to identify the outliers and then adjust them. This stage (denoted as Stage 1) is included the EVI-MMD algorithm and is done before the Adagrad optimization stage (denoted as Stage 2).

In Stage 1, given the initial particles, we first detect the outliers based on the driving force value. As discussed above, an outlier has a small driving force, so we detect the outlier according to the  $l_2$  norm,  $\|\text{driving}_i^n\|_2$ . With a pre-specified tolerance `tol`, we label a particle to be an outlier as long as  $\|\text{driving}_i^n\|_2 \leq \text{tol}$ . Once an outlier is detected, we adjust it by enlarging the size of the

driving force. Specifically, we force the driving force to have a pre-specified size  $\mathbf{a}$  while keeping the direction of the driving force, i.e.,

$$\text{driving}_i^n \leftarrow \mathbf{a} \frac{\text{driving}_i^n}{\|\text{driving}_i^n\|}.$$

Then, we update all particles using the explicit Euler scheme,  $\mathbf{x}_i^{n+1} = \mathbf{x}_i^n - \tau \mathbf{v}_i^n$ . So far we have set the two tuning parameters `tol` and `a` based on experience and trial-and-error. Generally, the `tol` should be around the same scale of the smallest norm of driving force and `a` should be around the median of the norms of the driving force of all particles. We fix the step size  $\tau$  throughout Stage 1 and it should be slightly larger than the initial learning rate  $\eta_0$  for the Adagrad optimization. The number of iterations of Stage 1 is denoted  $B$  and it is relatively small compared to the total number of iterations of both stages, denoted as `maxIter`. Since the purpose of the first stage is to quickly move the outliers to the high-density region, the way we choose  $\tau$  and  $B$  is reasonable intuitively and effective in practice.

*Remark 2.* The convergence issue caused by outliers, or more generally the initial distribution, has been identified in the literature before. [Arbel et al. \(2019\)](#) studied the convergence of the continuous MMD gradient flow using the forward Euler discretization. Using the continuous formulation, the authors proved that if  $\|\rho_t(\mathbf{x}) - \rho(\mathbf{x})\|_{\dot{H}^{-1}(\rho_t)} \leq C$  for all  $t > 0$ , then  $\mathcal{F}(\rho_t) \leq C/(C\mathcal{F}(\rho_0)^{-1} + 4t)$ . Here  $\|\cdot\|_{\dot{H}^{-1}(\rho_t)}$  is the weighted homogeneous  $H^{-1}$  norm. The details can be found in [Arbel et al. \(2019\)](#). Intuitively, this result implies that the convergence rate of the MMD depends on the “distance” between  $\rho_t$ , the current density function, and the target distribution  $\rho$ . However, as pointed out in [Arbel et al. \(2019\)](#), the condition for the convergence rate is difficult to guarantee even if the “distance” between the initial distribution  $\rho_0$  and the target distribution  $\rho$  is small. The outlying particles with a small driving force described above correspond to the case when the “distance” between the empirical distribution of the current particles and the target distribution is large. Therefore, the outliers can lead to slow convergence or even fail to converge to the target distribution. In [Arbel et al. \(2019\)](#), the author proposed to inject noise to improve the robustness of the algorithm to outliers, whereas we propose the remedy of manually pushing the particles to a region of the higher probability density of the target distribution.

We present the EVI-MMD approach with outlier detection and adjustment in [Algorithm 1](#). The algorithm requires a list of tuning parameters. As we have explained, we set the tuning parameters mostly based on intuition, experience, and experimentation, which is a common practice in nearly all VI methods. How to set the tuning parameters is worthy of further investigation in the future. An important detail in [Algorithm 1](#) is regarding the second for-loop (indexed by  $i$ ) through the particles in both Stage 1 and 2. Although written into a for-loop, all the particles can be updated simultaneously by array operation or parallel computing, and we have used array operation in our codes. The most computational costly step is in estimating the driving force for each particle in every iteration, which depends on the sample size  $L$  or  $M$ .

## 4 Numerical Examples

We demonstrate the performance of the proposed EVI-MMD algorithm through three examples. They cover three scenarios in which the target distribution is fully specified, partially specified up to the normalizing constant, and empirically specified through training data. The last scenario is shown by a generative learning model using EVI-MMD. We also compare the EVI-MMD with the Monte Carlo cubature for a numerical integration problem. Through three toy examples, we

---

**Algorithm 1** The EVI-MMD Algorithm with Adjustment to Outliers

---

**Require:**

- 1:  $N$ : total number of particles;  
 $B$ : number of iterations of Stage 1;  
 $h$ : bandwidth parameter of the Gaussian kernel function;  
 $L$ : the size of samples generated from  $\mathcal{N}(\mathbf{x}_i, h^2 \mathbf{I}_d)$ ;  
**maxIter**: the total number of iterations of both Stage 1 and 2;  
**tol**: tolerance for outlier detection;  
**a**: adjustment parameter of the driving force of outlier;  
 $\tau$ : step size of explicit Euler in Stage 1;  
 $\eta_0$ : initial learning rate of Adagrad in Stage 2;  
 $\rho_0$ : an initial distribution with support  $\Omega$  to generate initial particles.
  - 2: Generate initial particles  $\{\mathbf{x}_i^0\}_{i=1}^N$  from distribution  $\rho_0$ .  
*Stage 1: Initial Outlier Detection and Adjustment.*
  - 3: **for**  $n = 1 : B$  **do**
  - 4:   **for**  $i = 1 : N$  **do**
  - 5:     Calculate the terms representing driving and repulsive force in (23) and (24).
  - 6:     **if**  $\|\text{driving}_i^n\| \leq \text{tol}$  **then**
  - 7:        $\text{driving}_i^n \leftarrow \mathbf{a} \frac{\text{driving}_i^n}{\|\text{driving}_i^n\|}$ .
  - 8:     **end if**
  - 9:      $\mathbf{v}_i^n = \text{repulsive}_i^n - \text{driving}_i^n$
  - 10:     $\mathbf{x}_i^{n+1} = \mathbf{x}_i^n - \tau \mathbf{v}_i^n$
  - 11:   **end for**
  - 12: **end for**  
*Stage 2: Adaptive Gradient Euler.*
  - 13: **for**  $n = 1 : (\text{maxIter} - B)$  **do**
  - 14:   Reset the learning rate to  $\eta_0$ .
  - 15:   **for**  $i = 1 : N$  **do**
  - 16:     Calculate the terms representing driving and repulsive force in (23) and (24).
  - 17:      $\mathbf{v}_i^n = \text{repulsive}_i^n - \text{driving}_i^n$
  - 18:     Compute  $\eta_t$  using (17).
  - 19:      $\mathbf{x}_i^{n+1} = \mathbf{x}_i^n - \eta_t \mathbf{v}_i^n$ .
  - 20:   **end for**
  - 21: **end for**
-

compare EVI-MMD to three alternatives, the EVI-Im, SVGD, and the stochastic Langevin Monte Carlo (LMC) by [Welling and Teh \(2011\)](#).

#### 4.1 Toy Examples

We specify the following three target distributions of  $d = 2$  dimensions.

1. Star-shaped five-component Gaussian mixture distribution:

$$\rho(\mathbf{x}) = \frac{1}{5} \sum_{i=1}^5 N(\mathbf{x}|\boldsymbol{\mu}_i, \boldsymbol{\Sigma}_i),$$

where

$$\boldsymbol{\mu}_i = \begin{bmatrix} \cos\left(\frac{2\pi}{5}\right), & -\sin\left(\frac{2\pi}{5}\right) \\ \sin\left(\frac{2\pi}{5}\right), & \cos\left(\frac{2\pi}{5}\right) \end{bmatrix}^{i-1} \begin{bmatrix} 1.5 \\ 0 \end{bmatrix}, \quad \boldsymbol{\Sigma}_i = \begin{bmatrix} \cos\left(\frac{2\pi}{5}\right), & -\sin\left(\frac{2\pi}{5}\right) \\ \sin\left(\frac{2\pi}{5}\right), & \cos\left(\frac{2\pi}{5}\right) \end{bmatrix}^{i-1} \begin{bmatrix} 1, & 0 \\ 0, & 0.01 \end{bmatrix}.$$

2. Eight-component Gaussian mixture distribution:

$$\rho(\mathbf{x}) = \frac{1}{8} \sum_{i=1}^8 N(\mathbf{x}|\boldsymbol{\mu}_i, \boldsymbol{\Sigma}),$$

where  $\boldsymbol{\mu}_1 = (0, 4)$ ,  $\boldsymbol{\mu}_2 = (2.8, 2.8)$ ,  $\boldsymbol{\mu}_3 = (4, 0)$ ,  $\boldsymbol{\mu}_4 = (-2.8, 2.8)$ ,  $\boldsymbol{\mu}_5 = (-4, 0)$ ,  $\boldsymbol{\mu}_6 = (-2.8, -2.8)$ ,  $\boldsymbol{\mu}_7 = (0, -4)$ ,  $\boldsymbol{\mu}_8 = (2.8, -2.8)$ , and  $\boldsymbol{\Sigma} = \begin{bmatrix} 0.2, & 0 \\ 0, & 0.2 \end{bmatrix}$ .

3. Wave-shaped distribution:

$$\rho(\mathbf{x}) = C^{-1} \exp\left(-0.1x_1^2 - (x_2 - \sin(\pi x_1))^2\right).$$

Although the first two distributions are both Gaussian mixture distributions, the second distribution is more challenging since the effective support region for each Gaussian component is separated, unlike the star-shaped distribution. The wave-shaped distribution contains an unknown normalizing constant  $C$ . Different from the approaches using KL-divergence, the EVI-MMD does require the normalizing constant to calculate the driving force term (23). So we estimate  $C$  using the Newton-Cotes quadrature implemented in Mathematica by [Wolfram Research, Inc. \(2021\)](#), and the result is  $C \approx 9.93$ .

For all three toy examples, we set the size of the particles  $N = 200$ . The initial distribution is a standard 2-dimensional Gaussian distribution. All the algorithms under comparison are terminated at `maxIter`=1000 when we are sure they all have reached convergence. For the EVI-MMD algorithm, we set  $\tau = 1$ ,  $\eta_0 = 0.1$ ,  $h = 0.2$ ,  $B = 20$ , `tol` = 0.002,  $L = 200$ , and `a` = 1 by default. For the eight-component Gaussian mixture distribution, due to the separated effective support region, there are more outliers among the initial particles, so we set the `a` = 2 to accelerate the adjustment step. For the star-shaped distribution, we discover  $\tau = 0.5$  leads to a more stable decrease of the MMD. The tuning parameters of the other algorithms are specified as their respective optimal ones based on our experimentation and/or previous publications. For the EVI-Im and SVGD methods, we set  $\eta_0 = 0.1$  and  $h = 0.2$ . The tuning parameters of LMC are  $a = 0.1$ ,  $b = 1$  and  $c = 0.55$ .

The three rows of sub-figures in Figure 1 illustrate how the particles are moved by the EVI-MMD algorithm from the  $n = 5$  iteration, the  $n = 100$  iteration, and the last iteration when the algorithm is terminated. We can see that most of the particles have been aligned to the high-density



region (highlighted by the yellow color) around the 100th iteration. To compare the performance of EVI-MMD with EVI-Im, SVGD, and LMC algorithms, we compute the  $\text{MMD}^2$  or  $D^2(\mathcal{X}, F, K)$  in each iteration for all of the four methods. Note that the EVI-MMD algorithm does not need to compute the  $\text{MMD}^2$  if not for this comparison. Figure 2 shows the decay of the  $\text{MMD}^2$  within the first five seconds of all four algorithms. The LMC and EVI-MMD have the fastest decay of the  $\text{MMD}^2$  and perform equally well for the star-shaped and wave-shaped distributions. But LMC is less stable than EVI-MMD as the  $\text{MMD}^2$  of LMC fluctuates around zero in later iterations. For the most challenging case, the eight-component Gaussian mixture distribution, LMC is slightly better than EVI-MMD. The SVGD has the worst performance as its corresponding  $\text{MMD}^2$  does not converge to zero. SVGD was shown to be less effective when the target distribution has separated support regions as in Wang et al. (2021). In this example, the SVGD has missed several of the eight components of the Gaussian mixture.

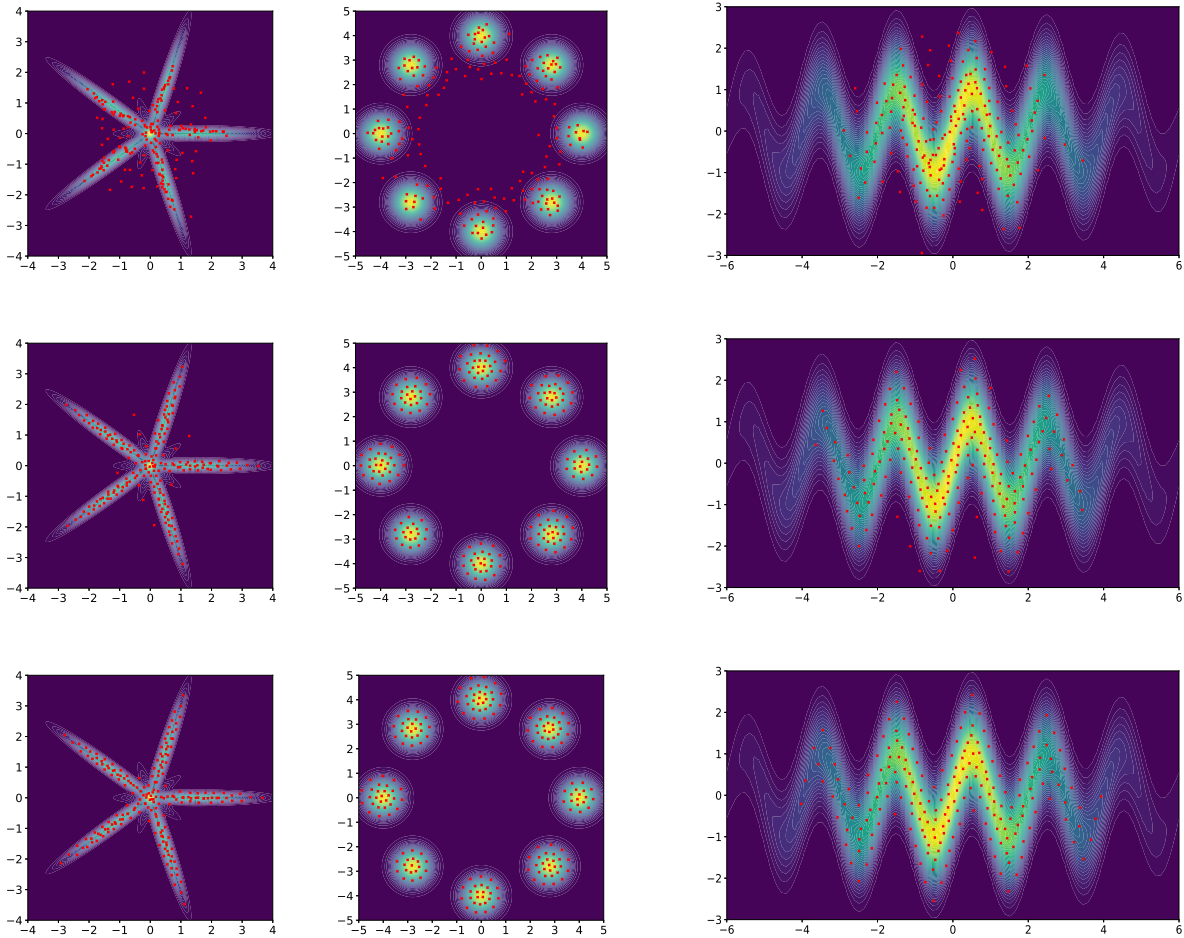


Figure 1: The particles generated by the EVI-MMD algorithm at  $n = 5$ ,  $n = 100$ , and  $n = 1000$  iterations in the three rows of the sub-figures, respectively, for the three target distributions.

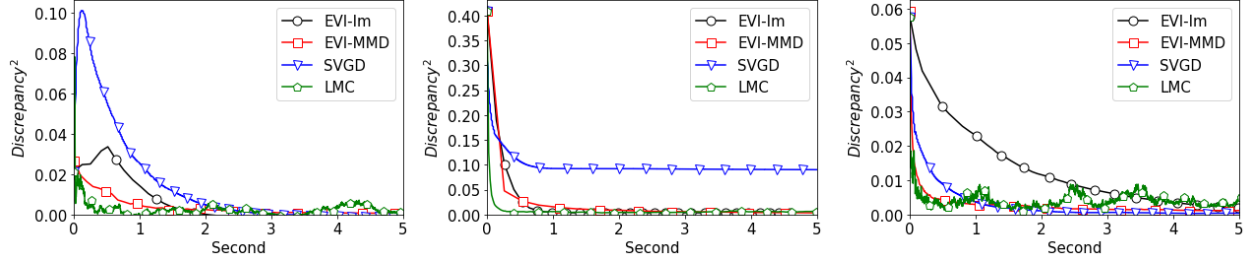


Figure 2: From left to right, the three sub-figures show the decreasing  $MMD^2$  in the first five seconds of the four algorithms under comparison for the star-shaped distribution, eight-component Gaussian mixture distribution, and the wave-shaped distribution.

## 4.2 Numerical Integration

As reviewed in Section 2.1, kernel discrepancy can be interpreted as part of the upper bound of the numerical integration error. So we demonstrate the performance of EVI-MMD through a numerical integration for Keister’s example given as follows.

$$I = \int_{\mathbb{R}^d} \cos(\|\mathbf{x}\|_2) \exp(-\|\mathbf{x}\|_2^2) d\mathbf{x}.$$

The exact integration can be calculated using the formula given in Jagadeeswaran and Hickernell (2019). Rounding up to four decimal digits, the integration values are  $I_{d=2} = 1.8082$  and  $I_{d=5} = 1.1353$  for  $d = 2$  and  $d = 5$  respectively. If using numerical integration, Keister’s integration can be easily computed using the classic Monte Carlo cubature. Rewrite the integration as follows

$$I = \int_{\mathbb{R}^d} \cos(\|\mathbf{x}\|_2) \exp(-\|\mathbf{x}\|_2^2) d\mathbf{x} = \int_{\mathbb{R}^d} \pi^{\frac{d}{2}} \cos \|\mathbf{x}/\sqrt{2}\|_2 \rho(\mathbf{x}) d\mathbf{x},$$

where  $\rho(\mathbf{x})$  is the pdf of a standard multivariate Gaussian distribution of  $d$  dimension. Then  $\hat{I}_N = \frac{1}{N} \sum_{i=1}^N \pi^{\frac{d}{2}} \cos \|\mathbf{x}_i/\sqrt{2}\|_2$  where  $\{\mathbf{x}_i\}_{i=1}^N$  are iid samples following  $\mathcal{MVN}(\mathbf{0}, \mathbf{I}_d)$ . The absolute relative error of the cubature is

$$\text{err}_r(f, \mathcal{X}) = \left| \frac{I - \hat{I}_N}{I} \right|, \quad \text{where } f(\mathbf{x}) = \pi^{\frac{d}{2}} \cos \|\mathbf{x}/\sqrt{2}\|_2.$$

We compare two approaches of generating random samples for the cubature. One is the classic Monte Carlo sampling that directly generates  $N$  samples from the Gaussian distribution. The other is the low-discrepancy points generated by the EVI-MMD method. The initial distribution of the EVI-MMD is a uniform distribution in  $[-1, 1]^d$ . The number of samples  $N$  is set the same for both approaches. For  $d = 2$ , we vary  $N$  from 50 to 250, and 100 to 500 for  $d = 5$ . The tuning parameters of EVI-MMD are set to be  $L = 200$ ,  $\tau = 0.05$ ,  $\eta_0 = 0.05$ ,  $B = 5$ ,  $\text{tol} = 0.001$ , and  $\mathbf{a} = 1$  for both dimensions. But  $h = 0.5$  for  $d = 2$  and  $h = 1.2$  for  $d = 5$ . Figure 3 compares the two methods with different sample sizes for  $d = 2$  and  $d = 5$ . For each  $N$ , we use a box plot to show the distribution of absolute relative errors of 20 replications of cubatures computed from 20 sets of samples. The EVI-MMD significantly outperforms the classic Monte Carlo for the cubature and has much less bias. Since it is essentially an optimization approach, the variance is very small as well.

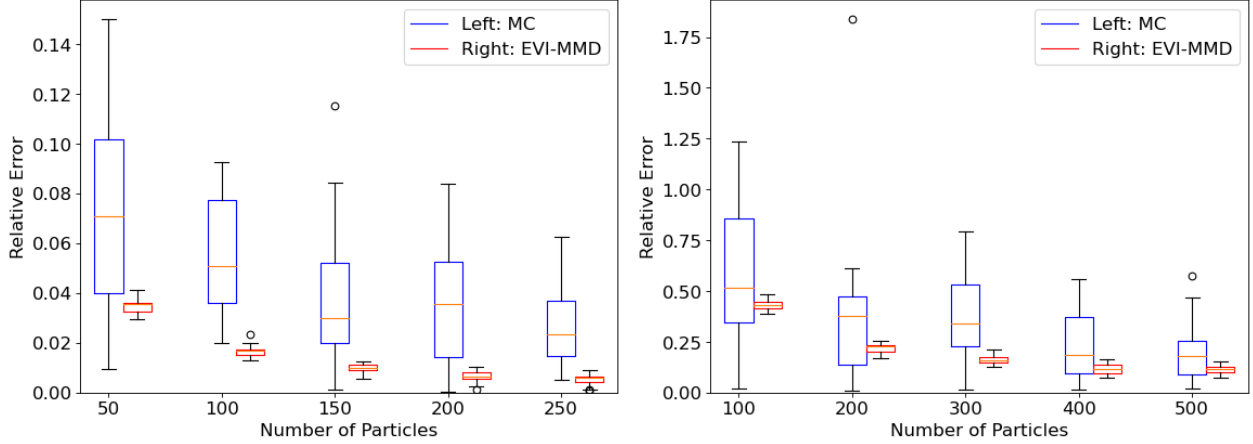


Figure 3: The absolute relative error of 20 replications of cubatures of the Keister’s example for  $d = 2$  (left) and  $d = 5$  (right) case.

### 4.3 Generative Learning Model

Generative learning models have been widely used in various machine learning applications. They can solve both supervised and unsupervised learning problems. Simply put, the generative learning model generates new samples based on the training data. More advanced generative learning models are combined with deep neural networks (Jabbar et al., 2021), Naive Bayes, Gaussian mixture model, hidden Markov model, etc. (Harshvardhan et al., 2020). In this example, we use the simplest nonparametric generative learning setup and apply the EVI-MMD to the famous benchmark MNIST dataset (LeCun et al., 1998).

Each data point in the MNIST dataset is a  $28 \times 28$  pixel image of a handwritten digit from 0 to 9 and a pixel value is in  $[0, 1]$ . For a simple demonstration, we randomly choose 1000 images from the entire MNIST dataset as the training data. Then we generate  $N = 100$  new images using the EVI-MMD approach. Essentially, this is a two-sample problem. In a certain sense, it is simpler than the previous examples as the driving force can be directly estimated from the training data using (18). On the other hand, this is not an easy problem because the dimension  $d = 28^2 = 784$  is extremely high considering the training data only has 1000 entries.

We specify the EVI-MMD as follows. The initial  $N = 100$  particles are sampled from a uniform distribution in  $[0, 1]^{784}$ . The other tuning parameters are set to  $\tau = 0.1$ ,  $\eta_0 = 0.05$ ,  $B = 20$ ,  $\text{tol} = 0.1$ ,  $\mathbf{a} = 10$ , and  $h = 1.1$ . We terminate the algorithm at  $\text{maxIter} = 30$  and the Adagrad converges in 10 iterations. The EVI-MMD does not need many iterations to decrease the  $\text{MMD}^2$  to nearly zero because each image is highly sparse. Figure 4 compares side-by-side the original 100 out of the 1000 training data and  $N = 100$  low-discrepancy points generated by EVI-MMD. Both the training and the low-discrepancy points are put into a  $10 \times 10$  panel. We can see that the digits generated by the EVI-MMD are similar to the training data. Note that the EVI-MMD is by no means the best approach for the MNIST benchmark example. Readers can find many more sophisticated generative learning approaches that return better results. However, the EVI-MMD is probably the simplest by comparison and its results are adequate.



Figure 4: Visual comparison between the 100 randomly sampled digits from the training data and 100 digits generated by the EVI-MMD.

## 5 Conclusion

In this paper, we develop a variational inference approach to generate low-discrepancy points to approximate a target distribution by minimizing the kernel discrepancy, alternatively known as maximum mean discrepancy (MMD). The minimization of MMD is solved by the general energetic variational inference (EVI) framework firstly introduced by Wang et al. (2021). Specifically, we use the quadratic dissipation functional of the EVI, apply the particle approximation to the continuous energy-dissipation law, which is then followed by the variation procedure. This leads to a dynamic system that moves the particles from their initial positions to the target distribution. Using the explicit Euler scheme to solve this dynamic system, we obtain a special algorithm based on the EVI framework to minimize MMD, which we call EVI-MMD algorithm.

Compared to the existing MMD-descent approaches, the EVI-MMD algorithm can be applied to different target distributions other than the two-sample problem. More importantly, if we change some settings of the EVI framework, new algorithms can be developed. For example, another possible dissipation functional is

$$\Delta_h = \dot{\mathbf{X}}^T \mathbf{A} \dot{\mathbf{X}}, \quad \mathbf{X} \in \mathbb{R}^{Nd} \text{ is the vectorized } \{\mathbf{x}_i\}_{i=1}^N, \quad (25)$$

where  $\mathbf{A} \in \mathbb{R}^{Nd \times Nd}$  is some positive-definite matrix. A simple case of  $\mathbf{A}$  is the circular convolution matrix

$$\mathbf{A} = \begin{bmatrix} 1+2\sigma & -\sigma & 0 & \dots & -\sigma \\ -\sigma & 1+2\sigma & -\sigma & \dots & 0 \\ 0 & -\sigma & 1+2\sigma & \dots & 0 \\ \dots & \dots & \dots & \dots & \dots \\ -\sigma & 0 & 0 & \dots & 1+2\sigma \end{bmatrix},$$

which corresponds to the Laplacian smoothing approach proposed in Osher et al. (2018). Potentially, this dissipation function can prevent the solution from being trapped at saddle points and local minimal. Some other dissipation functionals and numerical schemes for the EVI framework

are suggested in [Liu and Wang \(2020\)](#) and [Wang et al. \(2021\)](#). We will explore which EVI algorithm works most efficiently to minimize the MMD next.

A remaining issue for the EVI-MMD approach is how to specify the list of tuning parameters. Similar to many machine learning methods, we select the tuning parameters based on intuition and experimentation. A more systematic approach is called for and we plan to investigate this topic in the future.

## Acknowledgment

L. Kang's work is partially supported by the National Science Foundation Grant DMS-1916467. Y. Wang and C. Liu are partially supported by the National Science Foundation Grant DMS-1759536 and DMS-1950868.

## Appendix: Derivations and Extra Discussion

### A1 Derivations of (10) and (11)

Let  $\mathbf{x}_i^\epsilon = \mathbf{x}_i + \epsilon \mathbf{s}_i$  for any direction  $\mathbf{s}_i$ . We need to obtain the first order variation  $\frac{\delta \mathcal{F}}{\delta \mathbf{x}_i}$ . First we need to calculate

$$\begin{aligned} \left. \frac{d\mathcal{F}}{d\epsilon} \right|_{\epsilon=0} &= -\frac{2}{N} \int_{\Omega} \left. \frac{d}{d\epsilon} \right|_{\epsilon=0} K(\mathbf{x}_i^\epsilon, \mathbf{y}) dF(\mathbf{y}) + \frac{2}{N^2} \sum_{k \neq i}^N \left. \frac{dK(\mathbf{x}_i^\epsilon, \mathbf{x}_k)}{d\epsilon} \right|_{\epsilon=0} \\ &= -\frac{2}{N} \int_{\Omega} [\nabla_{\mathbf{x}} K(\mathbf{x}_i, \mathbf{y})]^\top \mathbf{s}_i dF(\mathbf{y}) + \frac{2}{N^2} \sum_{k \neq i} [\nabla_{\mathbf{x}} K(\mathbf{x}_i, \mathbf{x}_k)]^\top \mathbf{s}_i \\ &= -\frac{2}{N} \left[ \int_{\Omega} (\nabla_{\mathbf{x}} K(\mathbf{x}_i, \mathbf{y})) dF(\mathbf{y}) \right]^\top \mathbf{s}_i + \frac{2}{N^2} \sum_{k \neq i} [\nabla_{\mathbf{x}} K(\mathbf{x}_i, \mathbf{x}_k)]^\top \mathbf{s}_i. \end{aligned}$$

Therefore,

$$\frac{\delta \mathcal{F}}{\delta \mathbf{x}_i} = -\frac{2}{N} \int_{\Omega} [\nabla_{\mathbf{x}} K(\mathbf{x}_i, \mathbf{y})] dF(\mathbf{y}) + \frac{2}{N^2} \sum_{k \neq i} \nabla_{\mathbf{x}} K(\mathbf{x}_i, \mathbf{x}_k).$$

Similarly, for any direction  $\mathbf{s}_i$

$$\left. \frac{d\frac{1}{2}\Delta_h}{d\epsilon} \right|_{\epsilon=0} = \frac{1}{2N} \frac{d}{d\epsilon} (\dot{\mathbf{x}}_i + \epsilon \mathbf{s}_i)^\top (\dot{\mathbf{x}}_i + \epsilon \mathbf{s}_i) \Big|_{\epsilon=0} = \frac{1}{N} (\dot{\mathbf{x}}_i + \epsilon \mathbf{s}_i)^\top \mathbf{s}_i \Big|_{\epsilon=0} = \frac{1}{N} \dot{\mathbf{x}}_i^\top \mathbf{s}_i.$$

and

$$\frac{\delta \frac{1}{2}\Delta_h}{\delta \dot{\mathbf{x}}_i} = \frac{1}{N} \dot{\mathbf{x}}_i.$$

### A2 Discussion of the driving force term

We show that if a particle is an outlier, its corresponding driving force term would be small and thus make the algorithm stagnate. First, we give a rigorous definition of an outlier. Recall the driving force term is defined as (ignore the  $-$  sign)

$$\text{driving}_i = \int_{\Omega} - \left[ \frac{\mathbf{x}_i - \mathbf{y}}{h^2} \exp\left(-\frac{\|\mathbf{x}_i - \mathbf{y}\|_2^2}{2h^2}\right) \rho(\mathbf{y}) \right] d\mathbf{y}.$$

Given  $\epsilon > 0$ , define

$$S_1 := \{\mathbf{y} \mid \rho(\mathbf{y}) > \epsilon\}, \quad S_2 := \left\{ \mathbf{y} \mid \frac{\|\mathbf{x}_i - \mathbf{y}\|_\infty}{h^2} \exp\left(-\frac{\|\mathbf{x}_i - \mathbf{y}\|_2^2}{2h^2}\right) > \epsilon \right\}.$$

We introduce the following definition of  $\epsilon$ -outlier

**Definition A1.** A particle  $\mathbf{x}_i$  is an  $\epsilon$ -outlier if there exist a constant  $\epsilon$  such that  $S_1 \cap S_2 = \emptyset$ .

The support region  $\Omega$  can be split into three parts,  $S_1$ ,  $S_2$  and  $S_3 = (S_1 \cup S_2)^c$ . If  $\mathbf{x}_i$  is an  $\epsilon$ -outlier, we have  $S_3 = S_1^c \cap S_2^c$ . Accordingly, we can split the driving force term into integrals in these three regions and denote them as  $\mathbf{l}_{S_1}$ ,  $\mathbf{l}_{S_2}$  and  $\mathbf{l}_{S_3}$ .

**Proposition A1.** If a particle  $\mathbf{x}_i$  is an  $\epsilon$ -outlier, then the  $l_2$ -norm of the cross term satisfies,

$$\|\text{driving}_i\|_\infty \leq (C + 2)\epsilon \quad \text{and} \quad \|\text{driving}_i\|_2 \leq \sqrt{d}(C + 2)\epsilon,$$

where  $C = 2\pi^{d/2}/\Gamma(d/2)$  with  $\Gamma$  being the Gamma-function.

*Proof.* Apply the triangle inequality, we have

$$\|\text{driving}_i\|_\infty \leq \|\mathbf{l}_{S_1}\|_\infty + \|\mathbf{l}_{S_2}\|_\infty + \|\mathbf{l}_{S_3}\|_\infty.$$

Since the integration of  $\mathbf{l}_{S_1}$  is in  $S_1$  and  $S_1 \cap S_2 = \emptyset$ ,  $S_1 \subseteq S_2^c$

$$\|\mathbf{l}_{S_1}\|_\infty \leq \int_{S_1} \frac{\|\mathbf{x}_i - \mathbf{y}\|_\infty}{h^2} \exp\left(-\frac{\|\mathbf{x}_i - \mathbf{y}\|_2^2}{2h^2}\right) \rho(\mathbf{y}) d\mathbf{y} \leq \epsilon \int_{S_1} \rho(\mathbf{y}) d\mathbf{y} \leq \epsilon$$

Similarly, we can prove using the fact that  $S_2 \subseteq S_1^c$  and  $S_3 \subseteq S_2^c$ ,

$$\begin{aligned} \|\mathbf{l}_{S_2}\|_\infty &\leq \epsilon \int_{S_2} \frac{\|\mathbf{y} - \mathbf{x}_i\|_\infty}{h^2} \exp\left(-\frac{\|\mathbf{y} - \mathbf{x}_i\|_2^2}{2h^2}\right) d\mathbf{y} \leq \epsilon \int_{S_2} \frac{\|\mathbf{y} - \mathbf{x}_i\|_2}{h^2} \exp\left(-\frac{\|\mathbf{y} - \mathbf{x}_i\|_2^2}{2h^2}\right) d\mathbf{y} \leq C\epsilon \\ \|\mathbf{l}_{S_3}\|_\infty &\leq \int_{S_3} \frac{\|\mathbf{y}_j - \mathbf{x}_i\|_\infty}{h^2} \exp\left(-\frac{\|\mathbf{y} - \mathbf{x}_i\|_2^2}{2h^2}\right) \rho(\mathbf{y}) d\mathbf{y} \leq \epsilon, \end{aligned}$$

where  $C = 2\pi^{d/2}/\Gamma(d/2)$  with  $\Gamma$  being the Gamma-function. Following this result, if a particle is an  $\epsilon$ -outlier, then  $\|\text{driving}_i\|_\infty \leq (2 + C)\epsilon$ . Since  $\|\mathbf{x}\|_2 \leq \sqrt{d}\|\mathbf{x}\|_\infty$  for any  $\mathbf{x} \in \mathbb{R}^d$ , we have the upper bound for  $\|\text{driving}_i\|_2$ .  $\square$

## References

- Arbel, M., Korba, A., SALIM, A., and Gretton, A. (2019), “Maximum Mean Discrepancy Gradient Flow,” *Advances in Neural Information Processing Systems*, 32, 6484–6494.
- Ba, J., Erdogdu, M. A., Ghassemi, M., Suzuki, T., Sun, S., Wu, D., and Zhang, T. (2019), “Towards Characterizing the High-dimensional Bias of Kernel-based Particle Inference Algorithms,” in *2nd Symposium on Advances in Approximate Bayesian Inference*, pp. 1–17.
- Bernton, E. (2018), “Langevin Monte Carlo and JKO splitting,” in *Conference On Learning Theory*, pp. 1777–1798.
- Blei, D. M., Jordan, M. I., et al. (2006), “Variational inference for Dirichlet process mixtures,” *Bayesian analysis*, 1, 121–143.



- Blei, D. M., Kucukelbir, A., and McAuliffe, J. D. (2017), “Variational inference: A review for statisticians,” *J. Am. Stat. Assoc.*, 112, 859–877.
- Caffisch, R. E. (1998), “Monte carlo and quasi-monte carlo methods,” *Acta numerica*, 7, 1–49.
- Chen, C., Zhang, R., Wang, W., Li, B., and Chen, L. (2018a), “A unified particle-optimization framework for scalable bayesian sampling,” *arXiv preprint arXiv:1805.11659*.
- Chen, P., Wu, K., Chen, J., O’Leary-Roseberry, T., and Ghattas, O. (2019), “Projected Stein variational Newton: A fast and scalable Bayesian inference method in high dimensions,” in *Advances in Neural Information Processing Systems*, pp. 15130–15139.
- Chen, W. Y., Mackey, L., Gorham, J., Briol, F.-X., and Oates, C. (2018b), “Stein Points,” in *Proceedings of the 35th International Conference on Machine Learning*, eds. Dy, J. and Krause, A., PMLR, vol. 80 of *Proceedings of Machine Learning Research*, pp. 844–853.
- Cheng, C.-A. and Boots, B. (2017), “Variational Inference for Gaussian Process Models with Linear Complexity,” in *Advances in Neural Information Processing Systems 30*, eds. Guyon, I., Luxburg, U. V., Bengio, S., Wallach, H., Fergus, R., Vishwanathan, S., and Garnett, R., Curran Associates, Inc., pp. 5184–5194.
- Cheng, X., Chatterji, N. S., Bartlett, P. L., and Jordan, M. I. (2018), “Underdamped Langevin MCMC: A non-asymptotic analysis,” in *Conference on learning theory*, PMLR, pp. 300–323.
- Cheng, X. and Xie, Y. (2021), “Neural Tangent Kernel Maximum Mean Discrepancy,” *arXiv preprint arXiv:2106.03227*.
- Creswell, A., White, T., Dumoulin, V., Arulkumaran, K., Sengupta, B., and Bharath, A. A. (2018), “Generative adversarial networks: An overview,” *IEEE Signal Processing Magazine*, 35, 53–65.
- Csiszár, I., Shields, P., et al. (2004), “Information Theory and Statistics: A Tutorial,” *Foundations and Trends® in Communications and Information Theory*, 1, 417–528.
- Damianou, A. C., Titsias, M. K., and Lawrence, N. D. (2016), “Variational inference for latent variables and uncertain inputs in Gaussian processes,” *The Journal of Machine Learning Research*, 17, 1425–1486.
- Duchi, J., Hazan, E., and Singer, Y. (2011), “Adaptive subgradient methods for online learning and stochastic optimization,” *Journal of machine learning research*, 12.
- E, W., Ma, C., and Wu, L. (2020), “Machine learning from a continuous viewpoint, I,” *Science China Mathematics*, 1–34.
- Fang, K.-T., Lin, D. K., Winker, P., and Zhang, Y. (2000), “Uniform design: theory and application,” *Technometrics*, 42, 237–248.
- Fang, K.-T., Ma, C.-X., and Winker, P. (2002), “Centered  $L_2$ -discrepancy of random sampling and Latin hypercube design, and construction of uniform designs,” *Mathematics of Computation*, 71, 275–296.
- Fang, K.-T. and Mukerjee, R. (2000), “Miscellanea. A connection between uniformity and aberration in regular fractions of two-level factorials,” *Biometrika*, 87, 193–198.

- Fox, C. W. and Roberts, S. J. (2012), “A tutorial on variational Bayesian inference,” *Artificial intelligence review*, 38, 85–95.
- Fukumizu, K., Gretton, A., Sun, X., and Schölkopf, B. (2007), “Kernel measures of conditional dependence.” in *NIPS*, vol. 20, pp. 489–496.
- Giga, M.-H., Kirshtein, A., and Liu, C. (2017), “Variational Modeling and Complex Fluids,” in *Handbook of Mathematical Analysis in Mechanics of Viscous Fluids*, eds. Giga, Y. and Novotny, A., Springer International Publishing, pp. 1–41.
- Goodfellow, I., Pouget-Abadie, J., Mirza, M., Xu, B., Warde-Farley, D., Ozair, S., Courville, A., and Bengio, Y. (2014), “Generative adversarial nets,” *Advances in neural information processing systems*, 27.
- Gorbach, N. S., Bauer, S., and Buhmann, J. M. (2018), “Scalable variational inference for dynamical systems,” *Advances in Neural Information Processing Systems* 30, 7, 4807–4816.
- Graves, A. (2011), “Practical Variational Inference for Neural Networks,” in *Advances in Neural Information Processing Systems* 24, eds. Shawe-Taylor, J., Zemel, R. S., Bartlett, P. L., Pereira, F., and Weinberger, K. Q., Curran Associates, Inc., pp. 2348–2356.
- Gretton, A., Borgwardt, K. M., Rasch, M. J., Schölkopf, B., and Smola, A. (2012), “A kernel two-sample test,” *The Journal of Machine Learning Research*, 13, 723–773.
- Harshvardhan, G., Gourisaria, M. K., Pandey, M., and Rautaray, S. S. (2020), “A comprehensive survey and analysis of generative models in machine learning,” *Computer Science Review*, 38, 100285.
- Heng, J., Doucet, A., and Pokern, Y. (2021), “Gibbs flow for approximate transport with applications to Bayesian computation,” *Journal of the Royal Statistical Society: Series B (Statistical Methodology)*, 83, 156–187.
- Hickernell, F. (1998), “A generalized discrepancy and quadrature error bound,” *Mathematics of computation*, 67, 299–322.
- Hickernell, F. J. (1999), “Goodness-of-fit statistics, discrepancies and robust designs,” *Statistics & probability letters*, 44, 73–78.
- (2016), “The trio identity for Quasi-Monte Carlo error,” in *International Conference on Monte Carlo and Quasi-Monte Carlo Methods in Scientific Computing*, Springer, pp. 3–27.
- Hickernell, F. J. and Liu, M.-Q. (2002), “Uniform designs limit aliasing,” *Biometrika*, 89, 893–904.
- Hofert, M., Prasad, A., and Zhu, M. (2021), “Quasi-random sampling for multivariate distributions via generative neural networks,” *Journal of Computational and Graphical Statistics*, 1–24.
- Hu, Z., Yang, Z., Salakhutdinov, R., and Xing, E. P. (2018), “On Unifying Deep Generative Models,” in *International Conference on Learning Representations*.
- Jabbar, A., Li, X., and Omar, B. (2021), “A survey on generative adversarial networks: Variants, applications, and training,” *ACM Computing Surveys (CSUR)*, 54, 1–49.
- Jagadeeswaran, R. and Hickernell, F. J. (2019), “Fast automatic Bayesian cubature using lattice sampling,” *Statistics and Computing*, 29, 1215–1229.

- Jordan, M. I., Ghahramani, Z., Jaakkola, T. S., and Saul, L. K. (1999), “An introduction to variational methods for graphical models,” *Machine learning*, 37, 183–233.
- Jordan, R., Kinderlehrer, D., and Otto, F. (1998), “The variational formulation of the Fokker–Planck equation,” *SIAM journal on mathematical analysis*, 29, 1–17.
- King, N. J. and Lawrence, N. D. (2006), “Fast variational inference for Gaussian process models through KL-correction,” in *European Conference on Machine Learning*, Springer, pp. 270–281.
- Kingma, D. P., Mohamed, S., Jimenez Rezende, D., and Welling, M. (2014), “Semi-supervised learning with deep generative models,” *Advances in neural information processing systems*, 27, 3581–3589.
- Kingma, D. P., Salimans, T., Jozefowicz, R., Chen, X., Sutskever, I., and Welling, M. (2016), “Improved variational inference with inverse autoregressive flow,” in *Advances in neural information processing systems*, pp. 4743–4751.
- Kingma, D. P. and Welling, M. (2013), “Auto-encoding variational bayes,” *arXiv preprint arXiv:1312.6114*.
- LeCun, Y., Bottou, L., Bengio, Y., and Haffner, P. (1998), “Gradient-based learning applied to document recognition,” *proceedings of the IEEE*, 86, 2278–2324.
- Li, C.-L., Chang, W.-C., Cheng, Y., Yang, Y., and Póczos, B. (2017), “MMD GAN: towards deeper understanding of moment matching network,” in *Proceedings of the 31st International Conference on Neural Information Processing Systems*, pp. 2200–2210.
- Li, Y., Kang, L., and Hickernell, F. J. (2020), “Is a Transformed Low Discrepancy Design Also Low Discrepancy?” in *Contemporary Experimental Design, Multivariate Analysis and Data Mining*, Springer, pp. 69–92.
- Li, Y., Swersky, K., and Zemel, R. (2015), “Generative moment matching networks,” in *International Conference on Machine Learning*, PMLR, pp. 1718–1727.
- Liu, C. and Wang, Y. (2020), “A variational Lagrangian scheme for a phase-field model: A discrete energetic variational approach,” *SIAM Journal on Scientific Computing*, 42, B1541–B1569.
- Liu, C. and Zhu, J. (2017), “Riemannian Stein variational gradient descent for Bayesian inference,” *arXiv preprint arXiv:1711.11216*.
- Liu, C., Zhuo, J., Cheng, P., Zhang, R., and Zhu, J. (2019), “Understanding and Accelerating Particle-Based Variational Inference,” in *International Conference on Machine Learning*, PMLR, pp. 4082–4092.
- Liu, Q. (2017), “Stein variational gradient descent as gradient flow,” in *Advances in neural information processing systems*, pp. 3115–3123.
- Liu, Q., Lee, J., and Jordan, M. (2016), “A Kernelized Stein Discrepancy for Goodness-of-fit Tests,” in *Proceedings of The 33rd International Conference on Machine Learning*, eds. Balcan, M. F. and Weinberger, K. Q., New York, New York, USA: PMLR, vol. 48 of *Proceedings of Machine Learning Research*, pp. 276–284.
- Liu, Q. and Wang, D. (2016), “Stein variational gradient descent: A general purpose bayesian inference algorithm,” in *Advances in neural information processing systems*, pp. 2378–2386.

- Louizos, C. and Welling, M. (2017), “Multiplicative Normalizing Flows for Variational Bayesian Neural Networks,” in *Proceedings of the 34th International Conference on Machine Learning - Volume 70*, JMLR.org, ICML’17, p. 2218?2227.
- Ma, Y.-A., Chen, Y., Jin, C., Flammarion, N., and Jordan, M. I. (2019), “Sampling can be faster than optimization,” *Proceedings of the National Academy of Sciences*, 116, 20881–20885.
- Mak, S. and Joseph, V. R. (2018), “Support points,” *The Annals of Statistics*, 46, 2562–2592.
- Micchelli, C. A., Xu, Y., and Zhang, H. (2006), “Universal Kernels.” *Journal of Machine Learning Research*, 7.
- Mnih, A. and Rezende, D. J. (2016), “Variational inference for monte carlo objectives,” *arXiv preprint arXiv:1602.06725*.
- Nguyen, T. and Bonilla, E. (2013), “Efficient variational inference for Gaussian process regression networks,” in *Artificial Intelligence and Statistics*, pp. 472–480.
- Nguyen, T. V. and Bonilla, E. V. (2014), “Automated Variational Inference for Gaussian Process Models,” in *Advances in Neural Information Processing Systems 27*, eds. Ghahramani, Z., Welling, M., Cortes, C., Lawrence, N. D., and Weinberger, K. Q., Curran Associates, Inc., pp. 1404–1412.
- Onsager, L. (1931a), “Reciprocal relations in irreversible processes. I.” *Phys. Rev.*, 37, 405.
- (1931b), “Reciprocal relations in irreversible processes. II.” *Phys. Rev.*, 38, 2265.
- Osher, S., Wang, B., Yin, P., Luo, X., Barekat, F., Pham, M., and Lin, A. (2018), “Laplacian smoothing gradient descent,” *arXiv preprint arXiv:1806.06317*.
- Peyré, G., Cuturi, M., et al. (2019), “Computational optimal transport: With applications to data science,” *Foundations and Trends® in Machine Learning*, 11, 355–607.
- Rayleigh, L. (1873), “Some General Theorems Relating to Vibrations,” *Proceedings of the London Mathematical Society*, 4, 357–368.
- Rezende, D. J. and Mohamed, S. (2015), “Variational inference with normalizing flows,” *arXiv preprint arXiv:1505.05770*.
- Salman, H., Yadollahpour, P., Fletcher, T., and Batmanghelich, K. (2018), “Deep Diffeomorphic Normalizing Flows,” *arXiv preprint arXiv:1810.03256*.
- Shetha, R., Wangb, Y., Khardona, C. R., and EDU, T. (2015), “Sparse variational inference for generalized gaussian process models,” in *ICML*, pp. 1301–1311.
- Shridhar, K., Laumann, F., and Liwicki, M. (2019), “A comprehensive guide to bayesian convolutional neural network with variational inference,” *arXiv preprint arXiv:1901.02731*.
- Sobol, I. M. (1976), “Uniformly distributed sequences with an additional uniform property,” *USSR Computational Mathematics and Mathematical Physics*, 16, 236–242.
- Székely, G. J. and Rizzo, M. L. (2013), “Energy statistics: A class of statistics based on distances,” *Journal of statistical planning and inference*, 143, 1249–1272.

- Trillos, N. G. and Sanz-Alonso, D. (2020), “The Bayesian Update: Variational Formulations and Gradient Flows,” *Bayesian Analysis*, 15, 29 – 56.
- Villani, C. (2021), *Topics in optimal transportation*, vol. 58, American Mathematical Soc.
- Wang, D., Tang, Z., Bajaj, C., and Liu, Q. (2019), “Stein variational gradient descent with matrix-valued kernels,” *Advances in neural information processing systems*, 32, 7834.
- Wang, Y., Chen, J., Liu, C., and Kang, L. (2021), “Particle-based energetic variational inference,” *Statistics and Computing*, 31, 1–17.
- Welling, M. and Teh, Y. W. (2011), “Bayesian learning via stochastic gradient Langevin dynamics,” in *Proceedings of the 28th international conference on machine learning (ICML-11)*, pp. 681–688.
- Wibisono, A., Wilson, A. C., and Jordan, M. I. (2016a), “A variational perspective on accelerated methods in optimization,” *Proceedings of the National Academy of Sciences*, 113, E7351–E7358.
- (2016b), “A variational perspective on accelerated methods in optimization,” *proceedings of the National Academy of Sciences*, 113, E7351–E7358.
- Wolfram Research, Inc. (2021), “Mathematica, Version 12.3.1,” Champaign, IL, 2021.
- Wu, A., Nowozin, S., Meeds, E., Turner, R., Hernández-Lobato, J., and Gaunt, A. (2019), “Deterministic variational inference for robust Bayesian neural networks,” in *7th International Conference on Learning Representations, ICLR 2019*.
- Zhang, M., Bird, T., Habib, R., Xu, T., and Barber, D. (2019), “Variational f-divergence minimization,” *arXiv preprint arXiv:1907.11891*.